Available online at www.sciencedirect.com
ScienceDirect
Intermetallics 15 (2007) 1228–1236
Intermetallics
www.elsevier.com/locate/intermet

Tribological properties of graphite- and ZrC-reinforced bulk metallic glass composites

Marco E. Siegrist*, Esther D. Amstad, Jörg F. Löffler

Laboratory of Metal Physics and Technology, Department of Materials, ETH Zurich, Wolfgang-Pauli-Strasse 10, 8093 Zurich, Switzerland

Received 10 October 2006; received in revised form 20 February 2007; accepted 5 March 2007
Available online 30 April 2007

Abstract

The influence of second-phase reinforcement on the micro-tribological properties of $Zr_{52.5}Cu_{17.9}Ni_{14.6}Al_{10}Ti_5$ (Vit 105) was investigated by ball-on-disc tests. It was found that monolithic amorphous Vit 105 displays a coefficient of friction (COF) similar to that of 100Cr6 bearing steel. Further, it was seen that adding a low volume content of graphite and especially of ZrC generates a significant decrease in the COF, of up to 50%. Amorphous Vit 105 and its graphite-/ZrC-reinforced composites typically display two regimes of COF. After 100–500 revolutions it drops to about 2/3 of the starting value, and jumps back up to the initial COF are also observed. These transitions take place within the space of about 10 revolutions and are accompanied by a significant change in wear track depth. Investigation of the wear rate indicates that the graphite-/ZrC-reinforced bulk metallic glass composites display an even lower wear rate than 100Cr6 bearing steel.

Keywords: A. Composites; B. Tribological properties; B. Glasses, metallic; D. Phase interfaces; G. Wear-resistant applications

1. Introduction

Many amorphous metallic alloys with good glass-forming ability have been developed over the last few years (for reviews see Refs. [1–3]). Unfortunately, the high strength of these bulk metallic glasses (BMGs) cannot be fully exploited due to the alloys' brittle fracture behavior: they tend to deform along one or a few highly localized shear bands [4–8]. This has stimulated the development of many *in situ* [9–13] and *ex situ* [14–18] BMG composites, which have been shown to significantly improve the plastic strain of BMGs. The mechanical properties of these composites have been thoroughly investigated, but very little attention has so far been paid to their tribological features. Even those of monolithic amorphous alloys are not yet fully understood (for an overview, see Ref. [19]).

Due to the lack of plasticity in amorphous alloys, micro-cracking is considered to be their main wear mechanism [20]. Micro-cracking is more prevalent if crystals are present in the amorphous matrix, because these may act as crack nucleation sites. This is especially relevant because conventional metallic glasses have been shown to display local crystallization of the wear surface [21] and debris [22] due to frictional heat. BMGs have been described as displaying either worse [23] (especially under lubricated conditions) or better [24] wear resistance than commercial steel.

One way of altering the tribological properties of a system is to change its contact surface on a microscopic scale. In metallic glasses, the contact surface can be significantly influenced by adding second-phase particles which possess a different hardness than the amorphous matrix. We have chosen graphite as a reinforcement phase because of its superlubricity [25] and the potential for *in situ* formation of very hard ZrC particles in Zr-based BMGs [11]. In addition, graphite reinforcement of crystalline Al–Si alloys has been shown to significantly decrease both the coefficient of friction (COF) and the wear rate of the alloy at low contact loads [26].

In this contribution we compare the tribological properties of two different BMG composites (a $Zr_{52.5}Cu_{17.9}Ni_{14.6}Al_{10}Ti_5$

* Corresponding author. Tel.: +41 44 632 26 43; fax: +41 44 633 14 21.
E-mail address: marco.siegrist@mat.ethz.ch (M.E. Siegrist).

0966-9795/$ - see front matter © 2007 Elsevier Ltd. All rights reserved.
doi:10.1016/j.intermet.2007.03.001

(Vit 105)–graphite composite [18] and a novel three-phase composite with graphite and ZrC in a Vit 105 matrix) with those of the monolithic BMG and 100Cr6 bearing steel. We show that the COF of the metallic glass can be significantly decreased by adding the (graphite and ZrC) reinforcement phases. The low COF and the very high compressive yield strength (~1.8 GPa) of these composites make them potential candidates for self-lubricating friction-bearing materials.

2. Experimental

2.1. Processing

Pre-alloys with atomic composition $Zr_{52.5}Cu_{17.9}Ni_{14.6}Al_{10}Ti_5$ (Vit 105) were prepared in a Bühler AM system by arc-melting the high-purity elements (>99.95%) in a 300 mbar Ar 6.0 atmosphere. The subsequent composite preparation took place in a 1200 mbar Ar 6.0 atmosphere. Conducting-grade graphite of 2–13 vol.% with a particle size of 25–44 μm was induction-mixed with the pre-alloy in a water-cooled "silver boat". The crystalline composites were then suction-cast into 2 mm × 7 mm × 30 mm platelets in a Bühler MAM1 arc melter at a setting of 1 (0.35 kW) producing Vit 105–graphite composites, or at a setting of 2–3 (0.65–1.4 kW) producing Vit 105–graphite–ZrC composites (with the ZrC being present at the interface). Multiple remelting and suction-casting of these Vit 105–graphite–ZrC composites produced three-phase composites with graphite and ZrC present as particles in a Vit 105 matrix. Monolithic BMG samples were prepared without the induction mixing step, and one sample was fully crystallized by annealing at 430 °C for 75 min. Hardened 100Cr6 bearing steel (846 HV) was used as a reference sample.

2.2. Tribological characterization

The tribological properties of the material were investigated on a CETR micro-tribometer, where the sample was paired against a 100Cr6 bearing steel ball with a diameter of 2 mm at a constant sliding speed of 100 mm/min without lubrication. Before measurement all samples were ground and polished with a 0.05 μm Al_2O_3 dispersion.

The vertical force of the ball on the sample (F_z) was held constant during the test and the frictional force (F_x) and the change in track depth were recorded (see schema in Fig. 1). The COF was obtained by dividing the frictional force (F_x) by the vertical force (F_z). All tests were run at room temperature at a relative humidity of about 40%. First the ball was run in for 100 revolutions at a 5 N load. The test runs were performed with 100 revolutions at a 5 N load, and 10, 100 and 1000 revolutions at a 1 N load. No difference in tribological behavior was observed between tests performed at 5 N and at 1 N; thus only the tests performed at 1 N are presented here. The steel ball was run in at a radius of 2.9 mm and the radius was reduced by 0.4 mm for each of the subsequent tests, as seen in Fig. 2. The high COF regime was determined by approximating the force data obtained in the 100-revolution tests with an exponential relaxation function. In the steel sample the 1000-revolution data were used because the COF was not yet in equilibrium after 100 revolutions due to the steel sample's oxide layer. In samples displaying two COF regimes in the 1000-revolution tests, the lower was determined by averaging its values.

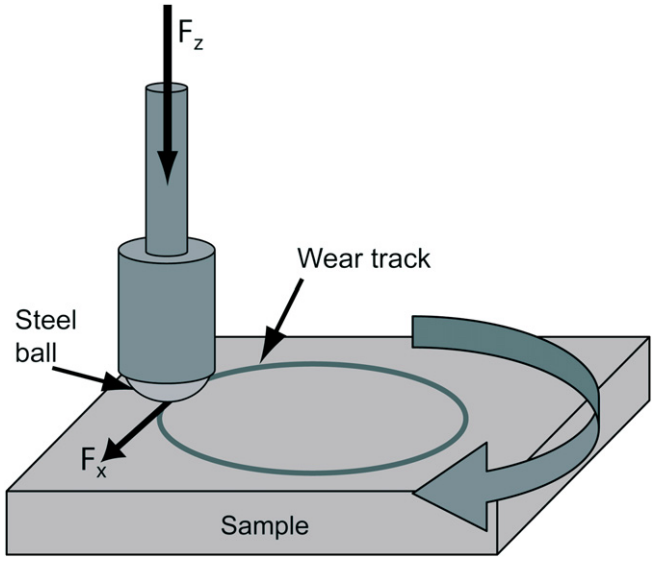

Fig. 1. Schema of the ball-on-disc tribometer used for micro-tribological investigation. A fixed bearing steel ball with a diameter of 2 mm is pressed on top of a rotating sample using a constant force (F_z). The frictional force (F_x) and the change in ball height were recorded.

2.3. Thermophysical and optical characterizations

The samples were further characterized by X-ray diffraction (PANalytical X'Pert diffractometer with Cu Kα radiation), energy dispersive X-ray diffraction (CamScan scanning electron microscope equipped with a Noran Energy Dispersive X-ray detector), high-resolution scanning electron microscopy (SEM) (Zeiss Gemini 1530 FEG), and optical microscopy (Reichert–Jung Polyvar Met microscope). The graphite volume content

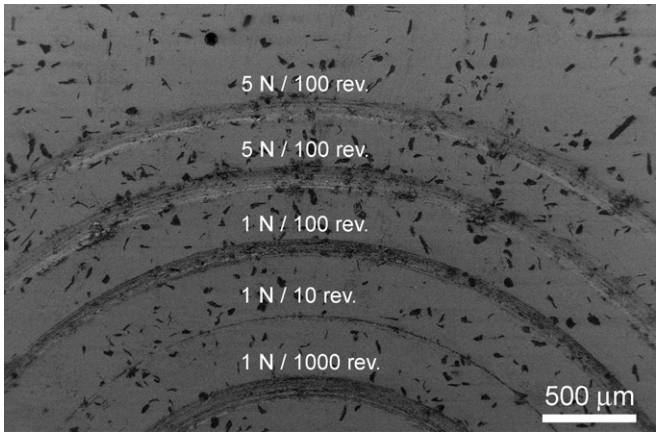

Fig. 2. SEM images giving an overview of the various wear tracks made on a Vit 105–graphite composite containing 8 vol.% graphite using different parameters.

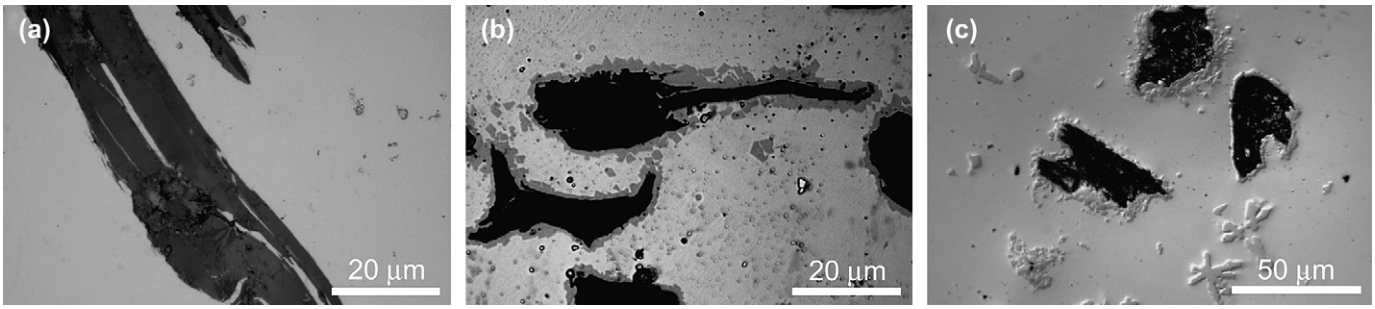

Fig. 3. Optical micrographs of (a) Vit 105–graphite composite; (b) Vit 105–graphite–ZrC composite (with only interfacial ZrC); and (c) three-phase composite (graphite and ZrC particles in a Vit 105 matrix).

of the tribological surfaces was determined by analyzing the optical micrographs (Leica QWin software).

3. Results

3.1. Microstructure of the various composites

The microstructure of graphite-reinforced BMG composites can be tailored by adjusting the processing parameters. As seen in Fig. 3a–c, we have produced three types of BMG composites: (a) Vit 105–graphite composites as described in Ref. [18], which show a clean graphite–matrix interface; (b) Vit 105–graphite–ZrC composites with an interfacial ZrC layer of about 2 µm (obtained by increasing the processing temperature in the final casting step); and (c) three-phase composites with graphite and ZrC particles in the Vit 105 matrix (obtained by multiple remelting and casting of Vit 105–graphite–ZrC composites). All the composites display a homogeneous particle distribution, as seen for example in Fig. 2.

Fig. 4 shows XRD scans of the three types of composites, all with 7 vol.% graphite. The Vit 105–graphite–ZrC composite and the three-phase composite display ZrC peaks of similar intensity, while the Vit 105–graphite composite displays almost no carbide formation. All composites show a significant amorphous background. The Vit 105–graphite composites and the three-phase composites were used for further tribological testing.

XRD scans were performed before and after tribological tests on a three-phase composite and a Vit 105–graphite composite with 3 and 4 vol.% graphite, respectively. No significant changes were seen before or after the tribological tests (not shown), suggesting that no crystallization of the wear track or debris took place.

3.2. Tribological properties

Fig. 5a–e show a comparison of the COF (black data) and wear trace depth (grey data) in 1000-revolution tests conducted with a 1 N load on (a) amorphous Vit 105; (b) crystalline Vit 105; (c,d) three-phase composites with 3 and 7 vol.% graphite; and (e) 100Cr6. All the samples tested for 1000 revolutions showed an increase in wear track depth, with the exception of amorphous Vit 105 (Fig. 5a), which showed a decrease in track depth due to agglomeration of debris between the steel ball and the wear track (pin-lifting phenomenon). Crystalline Vit 105 (Fig. 5b) and the three-phase composites (Fig. 5c and d) showed a more or less linear increase in track depth (with a similar increase of about 5 µm after 1000 revolutions), whereas the bearing steel (Fig. 5e) displayed a faster increase in track depth during the first 200 revolutions than during the remainder of the test. In contrast to the three-phase composites and crystalline Vit 105, the 100Cr6 steel showed a track depth of about 13 µm after 1000 revolutions. The fluctuations in wear track depth seen in 100Cr6 and crystallized Vit 105 in particular are due to the non-parallel installation of the samples in the testing rig, and are of no tribological significance, whereas the jumps in amorphous Vit 105 are related to the pin-lifting phenomenon.

It took about 200 revolutions at a load of 1 N for the 100Cr6 bearing steel sample to reach a steady COF state (see black data in Fig. 5e). This did not apply to the other tested materials, which all reached a steady state within <20 revolutions. The amorphous Vit 105 (Fig. 5a) and the three-phase composites (Fig. 5c and d) display two significant COF regimes. This is

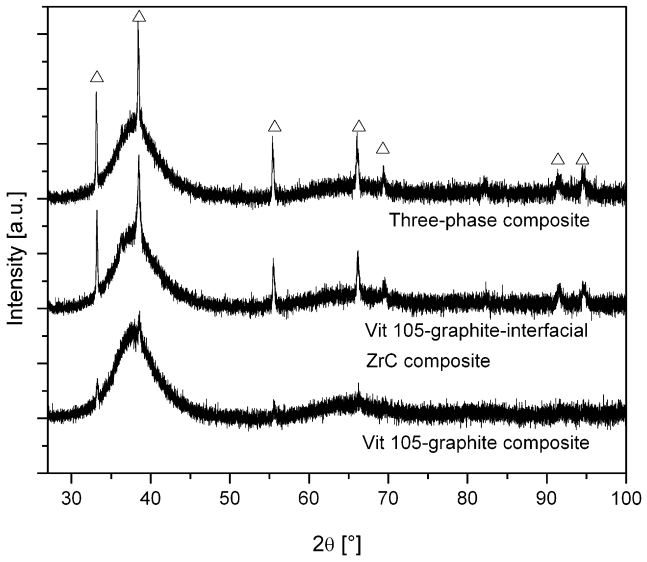

Fig. 4. XRD scans of the three composite types shown in Fig. 3: Vit 105–graphite composite; Vit 105–graphite–ZrC composite (with only interfacial ZrC formation); and three-phase composite (graphite and ZrC particles in a Vit 105 matrix) with 7 vol.% reinforcement.

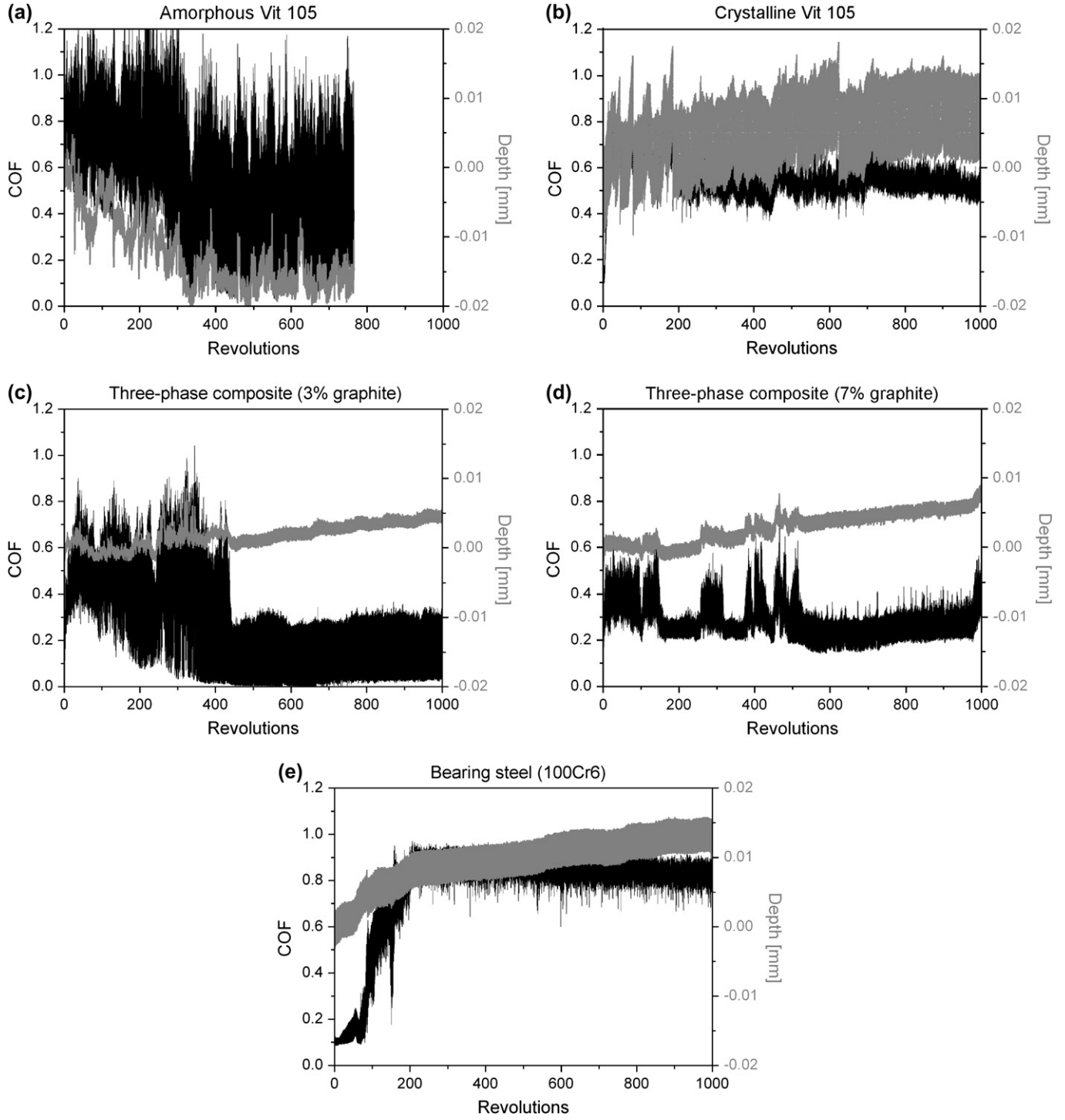

Fig. 5. COF (black) and pin height (grey) during 1000-revolution tests at 1 N load on (a) monolithic amorphous Vit 105; (b) fully crystalline Vit 105; (c) three-phase composite with 3 vol.% graphite; (d) three-phase composite with 7 vol.% graphite; and (e) 100Cr6 hardened bearing steel.

not the case for crystalline Vit 105 (Fig. 5b) or 100Cr6 (Fig. 5e). The samples showing two COF regimes are in the high regime at the beginning of the test and drop to the lower one after 100–400 revolutions. Jumps from the lower regime of COF to the higher regime were observed in the three-phase composites with more than 3 vol.% graphite, as shown in Fig. 5d.

The three-phase composites show smaller COF fluctuations in the lower regime than in the higher, whereas amorphous Vit 105 displays very high fluctuations in both regimes. Crystalline Vit 105 and 100Cr6 both display small fluctuations in COF. In general, it was found that the Vit 105–graphite composite and especially the three-phase composites showed smaller COF fluctuations with increasing graphite content.

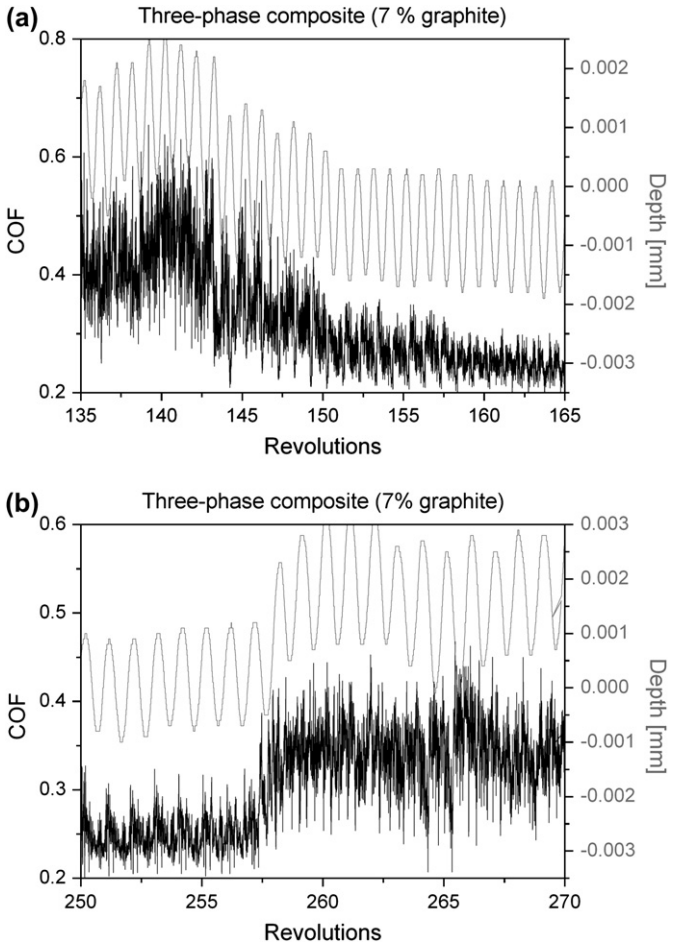

Fig. 6. Graph illustrating the transition from (a) high to low regime and (b) from low to high regime of COF (black) and the associated change in track depth (grey) for the three-phase composite with 7 vol.% graphite shown in Fig. 5d.

Sections with jumps from high to low and low to high regimes of the COF are shown in Fig. 6a and b, respectively, for the three-phase composite with 7 vol.% graphite (Fig. 5d). The jump from the high to low COF regime takes place within the space of about 10 revolutions, whereas the jump back up to the high regime takes place within about 2 revolutions. In both cases the jumps are accompanied by a significant change in track depth of about 2 μm. The track depth decreases when the COF drops and increases when the COF rises. The sinusoidal waveform of the wear track depth curve with a period of 1 revolution reflects the alignment of the sample in the tribometer.

Fig. 7 shows the COF measured in 100-revolution tests using a load of 1 N for (a) amorphous Vit 105; (b) crystalline Vit 105; (c) Vit 105–graphite composite with 8 vol.% graphite; and (d) three-phase composite with 8 vol.% graphite. The raw data (black) was approximated by an exponential relaxation function (grey). It can be seen that amorphous Vit 105 (Fig. 7a) displays the highest COF, followed by crystalline Vit 105 (Fig. 7b) and the Vit 105–graphite composite (Fig. 7c), which display similar values, and the three-phase composite (Fig. 7d), which has the lowest COF. As in the 1000-revolution tests, amorphous Vit 105 displays large fluctuations in the COF compared to crystalline Vit 105 and the three-phase composite. The Vit 105–graphite composite displays fluctuations similar to those of monolithic amorphous Vit 105.

Fig. 8 gives an overview of the COF–graphite content relationship for Vit 105–graphite composites and three-phase composites at a load of 1 N. The high and low regimes of friction were determined from the 100- and 1000-revolution tests, respectively. In the high COF regime the amorphous monolithic alloy shows a COF of about 0.8, which is comparable to that measured for the 100Cr6 bearing steel (0.78). As seen in Fig. 8, the reinforcement of the monolithic glass with very low volume contents of graphite generates a significant decrease in COF, especially in the case of the three-phase composites, which show about twice the decrease in COF than seen in the Vit 105–graphite composites for the same reinforcement fraction. In the lower regime of friction, monolithic Vit 105 displays a COF of about 0.48. A reinforcement content of only 3 vol.% graphite generates a decrease of COF to about 0.15 in the three-phase composite, while the three-phase composites with 7, 8 and 9 vol.% graphite show a slightly higher COF of about 0.23. In the tests conducted with a 5 N load (not shown), only the higher regime of friction was investigated, because no 1000-revolution tests were performed and no significant difference in the effect of graphite reinforcement was observed compared to the tests run at a 1 N load.

Fig. 9 shows SEM images of the three-phase composites after the tribological tests. A few shear bands were found at the edge of the wear tracks after 1000 revolutions at a 1 N load, as can be seen in Fig. 9a. The shear bands, which give evidence of high stress leading to inhomogeneous flow, run about 25° to the sliding direction. In some of the composite samples smeared matrix material was found in the wear track, as shown in Fig. 9b. This probably comes from deformation in the undercooled liquid region caused by local frictional heating and shear in the wear tracks. No micro-cracking was observed in the wear tracks of any of the tested materials.

In general, very little smearing of graphite was observed in the composite samples. We found by SEM investigation of 1 N wear tracks that entire graphite particles were torn from the 1000-revolution tracks but not from the 100-revolution tracks, meaning that the first particles came out after >100 revolutions. Fig. 10a shows the hole left by a graphite particle torn from a composite sample after 1000 revolutions at a 1 N load. A lot of debris is visible in the hole. The three-phase composite samples show several channels in their wear tracks, as seen in Fig. 10b. The depth of these channels is estimated to be about 3 μm. Fig. 10c shows the surface of the steel ball after a complete test on a three-phase composite. Several small particles with a size between 50 and 500 nm were found on the surface of the steel ball, and are thought to be ZrC debris because they were only observed after tribological tests on the three-phase composites.

A comparison of the width and depth of the wear tracks provides a qualitative approximation of the wear rate. The narrowest wear track, of about 50 μm after 1000 revolutions at a 1 N load, was seen for crystalline Vit 105, and the widest, of about 200 μm, for the hardened steel. No significant difference was detected between those of amorphous Vit 105 and its

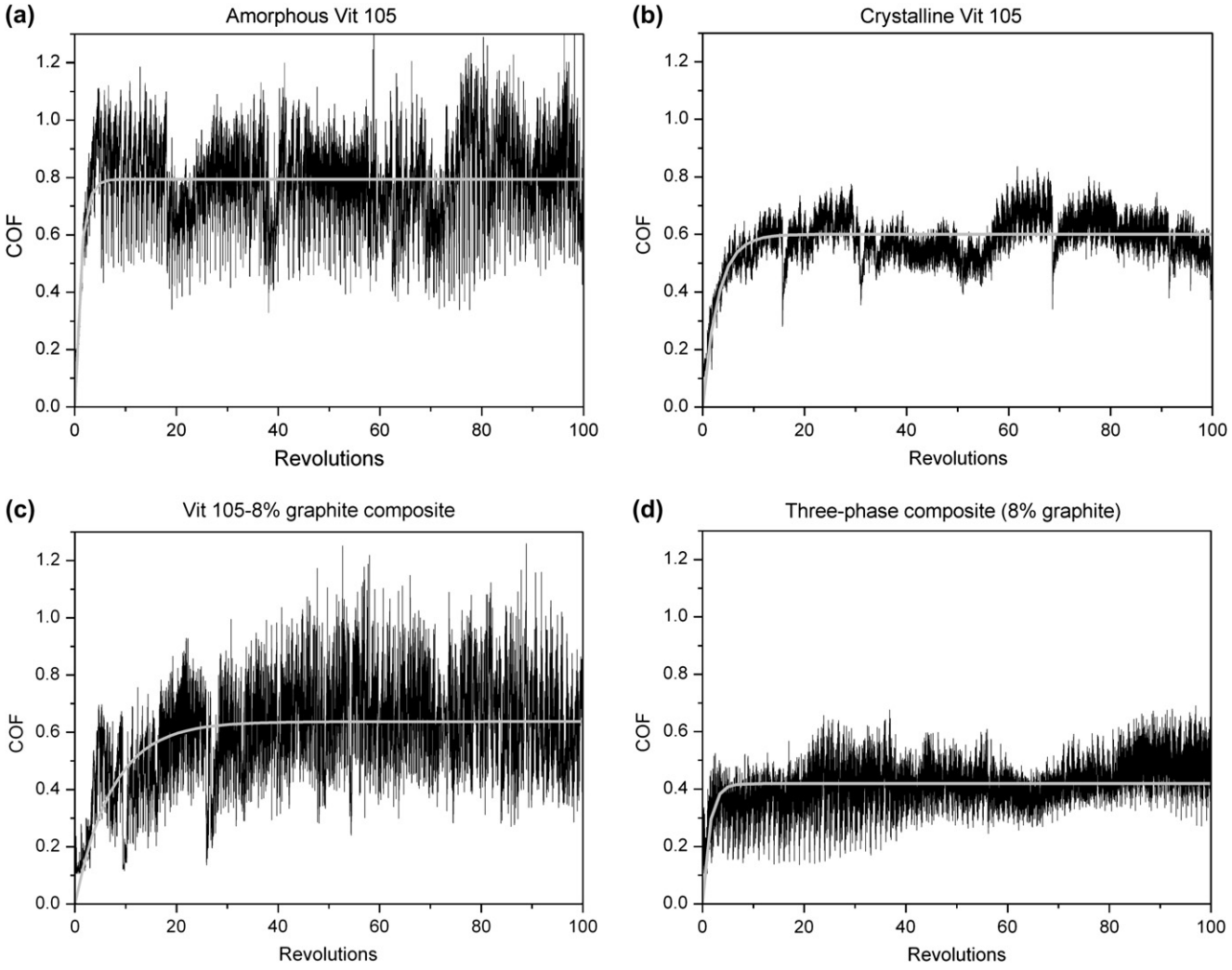

Fig. 7. COF during 100-revolution tests for (a) monolithic amorphous Vit 105; (b) crystalline Vit 105; (c) Vit 105–graphite composite with 8 vol.% graphite; and (d) three-phase composite with 8 vol.% graphite. The raw data were approximated with an exponential relaxation function (grey curve) to determine the COF.

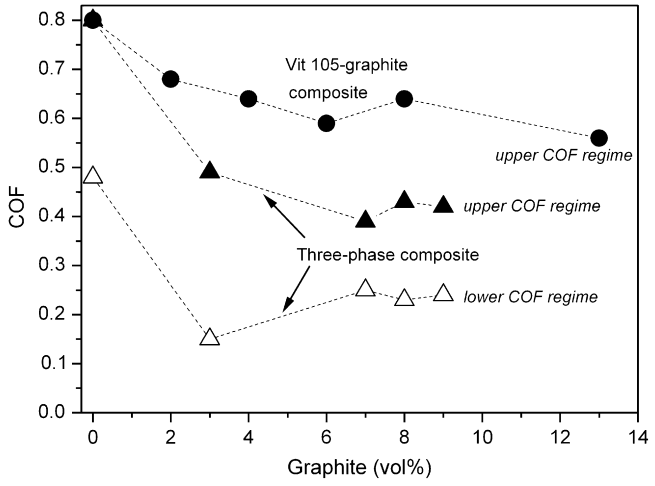

Fig. 8. COF as a function of graphite content for Vit 105–graphite composites and three-phase composites. The upper and lower regimes of COF are shown for the three-phase composites.

composites, which all displayed track widths of about 120 μm. The depths of the wear tracks are difficult to compare because of the observed pin-lifting phenomena in amorphous Vit 105. However, we found that the wear tracks of the three-phase composites after 1000 revolutions at a load of 1 N are less deep than those of the bearing steel, as shown in Fig. 5c–e and confirmed by SEM analysis. The depths and widths of the wear tracks do not correlate with the hardness values of the monolithic materials, which are 846 HV, 547 HV and 478 HV for the bearing steel and crystalline and amorphous Vit 105, respectively.

4. Discussion

4.1. Tailoring of composite microstructure

We have shown that the microstructure of the graphite-reinforced BMG composites can be tailored by adjusting their processing parameters. The literature reports that ZrC can be

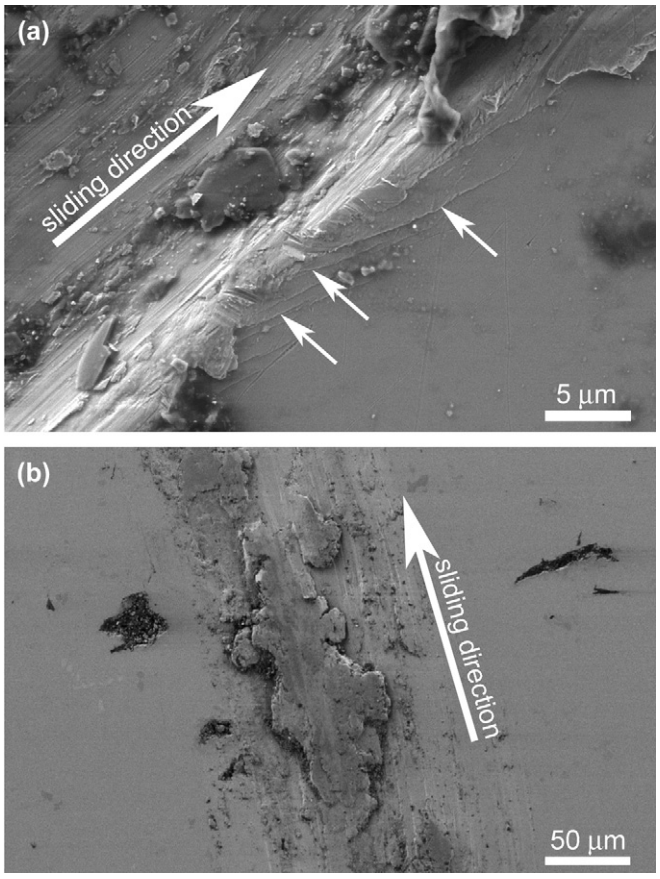

Fig. 9. SEM images of wear traces in three-phase composites showing (a) shear bands (marked by arrows) on the edge of the wear traces and (b) smearing of matrix material after 1000 revolutions at 1 N.

formed by adding small graphite particles to a Zr-based BMG, leading to *in situ* composite formation [11,27,28]. By using larger graphite particles (>25 µm instead of the typical <10 µm for *in situ* composite formation) and adjusting the processing temperature we can develop Vit 105–graphite composites (Fig. 3a) without an interfacial reaction, or Vit 105–graphite–ZrC composites (Fig. 3b) with interfacial carbide formation.

The three-phase composites shown in Fig. 3c are produced by multiple remelting and suction-casting of the composites with interfacial carbides through a defined nozzle. We believe that part of the interfacial ZrC is torn from the graphite particles by the suction-casting process due to the high flow rate of the melt through the nozzle, and that it is distributed homogeneously within the melt. Multiple repetition of this procedure generates a higher ZrC content in the matrix. Even though the ZrC formation causes depletion of Zr in the matrix, these composites still display an amorphous matrix at a casting thickness of 2 mm, as shown in the XRD results of Fig. 4.

4.2. Frictional properties of Vit 105

In the high COF regime, amorphous Vit 105 displays a similar COF to 100Cr6 bearing steel (see Fig. 5a and e); however, the metallic glass shows much stronger fluctuations. These are due to the stick-slip of the steel ball on the metallic glass. Stick-slip is common in materials where the static COF is significantly higher than the kinetic COF. We observed this in a Vit 105 sample by placing it on a steel plate and varying the incline. A very steep slope was needed to initiate the sliding of the sample, but, once it was in motion a much smaller incline was sufficient for it to continue. In amorphous Vit 105, the stick-slip observed may also be attributed to the special mechanical properties of the metallic glass. Because of the low stiffness and high elasticity of metallic glasses, the glassy Vit 105 alloy is expected to have a higher surface roughness than bearing steel or crystalline Vit 105 after grinding and polishing. Additionally, in an elastic, high-strength material the steel ball may be increasingly hindered by edges in the wear track, whereas in materials displaying little elasticity or low strength these edges will be worn off. Thus both effects support the observed stick-slip phenomenon.

There are two possible explanations for the pin-lifting phenomenon, observed especially in the high COF regime in amorphous Vit 105 (see Fig. 5a). First, debris accumulated in the wear track may get stuck between the steel ball and the amorphous matrix, lifting the steel ball off the wear surface. Second, local material smearing may lead to the material pile-up observed mainly on the edges of the wear tracks (as shown in Fig. 9a for a composite sample). This material pile-up looks like a decrease in wear track depth on a macroscopic scale. Such smearing is expected to take place in the undercooled liquid region, which is extensive in the matrix material [29] and even greater than in the monolithic alloy, because graphite addition leads to an increase in the crystallization temperature

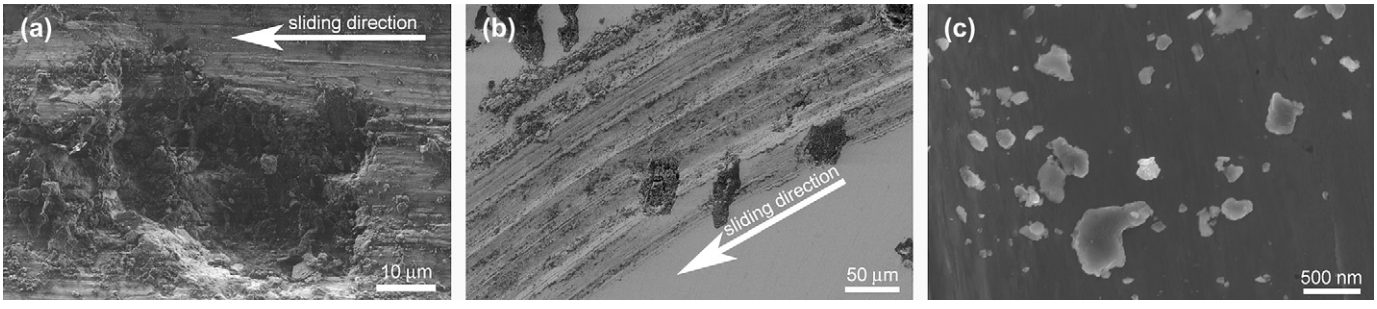

Fig. 10. SEM images showing (a) holes left by ripped-out graphite particles found in all three-phase composites after 1000 revolutions at a 1 N load; (b) channels in the wear tracks of three-phase composites; and (c) small ZrC particles found on the steel ball used for the wear tests of the three-phase composites.

[18]. Due to the very low sliding speed the smeared material is cooled by heat transfer to the bulk of the sample before the next revolution takes place. The cooling rate appears fast enough to hinder local crystallization: in contrast to observations of conventional metallic glasses [21,22], we found no hint of crystallization in the wear track or debris in any of the samples tested by XRD or micro-hardness measurements. In addition, if the wear surface layer did crystallize during sliding we would not observe material smearing, but a much more brittle abrasion behavior, as observed in crystalline Vit 105.

The local stress on the sample during the tribological tests can be very great, even exceeding the yield stress of the matrix. This renders plausible the large amount of matrix material smearing. If we consider the contact surface to be a circle with the diameter of the wear track (120 μm), the global stress would be about 90 MPa at a 1 N load. If, however, we further consider that very small debris may lie between the ball and the sample, the contact surface decreases significantly, generating very high local stress which could easily exceed the flow stress of the matrix material (about 1.9 GPa at room temperature). This further supports the possibility of deformation in the undercooled liquid region. Such high stresses also explain the shear banding observed next to the wear track, as shown for the three-phase composite in Fig. 9a. In this region inhomogeneous deformation (shear banding) is favored because no direct frictional heating takes place and the material temperature lies well below the glass transition temperature (T_g). Homogeneous deformation, in contrast, is more prevalent in the frictionally heated wear track, where the temperature is estimated to rise locally above T_g, allowing deformation at lower stresses (work softening). In contrast to the mechanism in metallic glasses, in 100Cr6 a decrease in the apparent wear track depth rate is observed after about 200 revolutions (see Fig. 5e). This is attributed to work hardening of the steel, leading to a more wear-resistant surface.

The two regimes of COF observed in the 1000-revolution tests for amorphous Vit 105 are clear evidence of two different sliding mechanisms. They may be attributed to the geometrical particularities of the sliding contact between the steel ball and the metallic glass in the micro-tribological experiments, as shown in Fig. 11. Within our model the ball plows through debris and rough edges in the wear track in the high COF regime, whereas in the low COF regime the ball is lifted onto the smeared material piled up on the edges of the track. This leads to a smaller contact area, reducing plowing and the adhesive component of friction (see also Ref. [30]). This model can also explain the apparent decrease in wear track depth associated with the drop in the COF. The COF in the low regime of friction is slightly lower than what we observed for crystalline Vit 105, which, like 100Cr6, displays no COF jumps.

4.3. Influence of reinforcement phases on frictional properties

As we have shown, reinforcement of Vit 105 leads to a significant change in tribological behavior. Graphite reinforcement generates a significant decrease in COF (see Fig. 8).

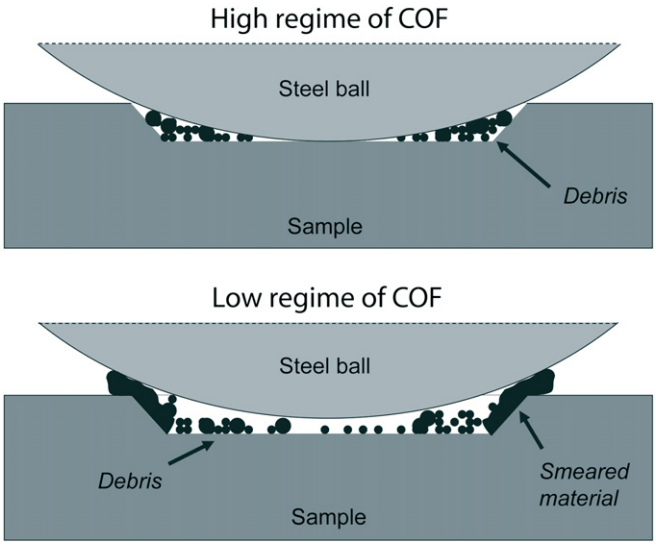

Fig. 11. Schema of steel ball on wear sample during tribological testing for the high and low COF regimes.

Graphite is known to lower the COF of tribological partners in metallic [26] and polymer-based [31] materials. In metallic systems, graphite sticks especially well to oxidized surfaces [25] (present on the surface of Zr-based BMGs [32] and steel). If graphite sticks to the surfaces of both tribological partners, graphite actually slides on graphite on a microscopic scale, which produces a very low COF. We also observed that debris was pushed into the soft graphite particles or the holes left by ripped-out particles (see Fig. 10a). This is expected to cause less abrasive wear and to additionally lower the COF.

The three-phase composites were also tested for 1000 revolutions at a 1 N load (see Fig. 5c and d) and also display two regimes of COF as observed for amorphous Vit 105. Thus we expect a similar ball-lifting mechanism to take place. In comparison to the monolithic amorphous alloy, we have shown that reinforcement of Vit 105 with graphite and ZrC (three-phase composites) leads to an even stronger decrease of the COF in the high and low regimes (see Fig. 8). In the regime of high COF strong fluctuations are present. This was also observed for the monolithic matrix material and Vit 105–graphite composites, which indicates that their sliding mechanism is similar. However, once the COF drops to the lower regime the COF fluctuations decrease drastically, which does not happen in amorphous Vit 105. This may be due to the hard ZrC debris, generating a smoother wear surface than in the monolithic alloy.

The multiple-channel morphology of the wear tracks observed in the three-phase composites shown in Fig. 10b contrasts with the single channel wear tracks found in Vit 105–graphite composites or the monolithic matrix material (not shown). Due to the very high strain rates achieved on a microscopic scale during sliding ($\sim 10^5\ s^{-1}$) it is unlikely that the multiple channels are formed by inhomogeneous deformation of the matrix material but rather by local abrasion of the matrix material by ZrC debris. Very small particles, probably ZrC debris, were found on the steel ball used for these tests (see Fig. 10c). It is probable that larger ones were also present but fell away due to their lower surface-to-weight ratio. Once a shallow channel

has formed, debris will remain in the channel and cause local abrasion, deepening it. The lower COF observed in the three-phase composites compared to Vit 105–graphite composites is probably due to the special geometry of the wear tracks, which generate a less extensive contact surface between the steel ball and the composites. The smaller contact surface has two effects: first, it reduces the adhesive component of friction between the steel ball and the composite; second, it produces higher local stress in the sliding contact, which may cause a smoothing of the sliding surface. The COF in the three-phase composites may be further reduced by bearing-like behavior on the part of the small, round carbide debris particles (see Fig. 10c) in the multiple channels of the wear track.

The fact that a very low reinforcement content is sufficient to lower the COF in both types of composite is a further evidence that the mechanisms are not based on the bulk material pairing, but rather on the influence of second-phase debris on dynamic contact during sliding. In both composites graphite acts as a lubricant and a debris trap. In the three-phase composites, ZrC debris also generates multiple-channel formation, drastically changing the sliding contact of the tribological system.

4.4. Wear rate

In contrast to Ref. [20], we observed no micro-cracking in the wear tracks of any of the amorphous materials. This supports the idea that the main wear mechanism in amorphous Vit 105 is the plowing of the amorphous material in the undercooled liquid region, and the additional tearing out of reinforcement particles in the Vit 105 composites.

Due to various wear mechanisms which produce different wear track morphologies it is very difficult to compare the wear rates of the materials investigated. However, an analysis of the data from the 1000-revolution tests and the SEM images taken thereafter shows that the width of the wear tracks and the measured depths of the wear traces are smaller in the three-phase composites than in 100Cr6 bearing steel. This is evidence that the wear rate of the newly developed three-phase composites is, in the micro-tribological testing setup used, lower than that of commercial bearing steel. This is due at least partially to the self-lubricating effect of graphite and the debris deposited on the holes left by torn-out graphite particles, both of which may generate less abrasive wear.

5. Conclusions

The microstructure of graphite-reinforced Vit 105 can be tailored by adjusting the processing parameters. This procedure also led to the development of a novel three-phase composite with graphite and ZrC in a fully amorphous Vit 105 matrix (as confirmed by XRD).

It was found that amorphous Vit 105 and all of its composites display two regimes of COF, and that the COF in the lower regime drops to about 2/3 of its initial value. This phenomenon was not observed either in crystalline Vit 105 or in bearing steel. The presence of two COF regimes was explained by an alteration in the wear track geometry via smearing of the matrix material in the undercooled liquid region. We also found that graphite and especially ZrC reinforcement generate a significant decrease in the COF of up to 50% compared to the monolithic alloy.

A qualitative comparison of the wear rate provides evidence that the graphite–ZrC composites developed in this study show even lower wear rates than commercial 100Cr6 bearing steel used as a reference material. These improved tribological properties and the high yield strength of the composites make them promising candidates for dry-frictional bearing material.

Acknowledgements

The authors would like to thank Roman Heuberger, Erwin Fischer and Christian Wegmann of the ETH Zurich, Switzerland for their technical support. Start-up funds from the ETH Zurich are also gratefully acknowledged.

References

[1] Johnson WL. MRS Bull 1999;24:42.
[2] Inoue A. Acta Mater 2000;48:279.
[3] Löffler JF. Intermetallics 2003;11:529.
[4] Spaepen F. Acta Mater 1976;25:407.
[5] Johnson WL, Lu J, Demetriou MD. Intermetallics 2002;10:1039.
[6] Sergueeva AV, Mara NA, Kuntz JD, Lavernia EJ, Mukherjee AK. Philos Mag 2005;85:2671.
[7] Liu LF, Dai LH, Bai YL, Wei BC, Eckert J. Mater Chem Phys 2005;93:174.
[8] Pekarskaya E, Kim CP, Johnson WL. J Mater Res 2001;16:2513.
[9] Hays CC, Kim CP, Johnson WL. Phys Rev Lett 1999;84:2901.
[10] Wang WH, Bai HY. Mater Lett 2000;44:59.
[11] Chen F, Takagi M, Imura T, Kawamura Y, Kato H, Inoue A. Mater Trans JIM 2002;43:1.
[12] Kühn U, Eckert J, Mattern N, Schultz L. Mater Sci Eng A 2004;375–377:322.
[13] Inoue A, Zhang W, Tsurui T, Yavari AR, Greer AL. Philos Mag Lett 2005;85:221.
[14] Choi-Yim H, Johnson WL. Appl Phys Lett 1997;71:3808.
[15] Choi-Yim H, Busch R, Köster U, Johnson WL. Acta Mater 1999;47:2455.
[16] Choi-Yim H, Conner RD, Szuecs F, Johnson WL. Acta Mater 2002;50:2737.
[17] Xu YK, Xu J. Scripta Mater 2003;49:843.
[18] Siegrist ME, Löffler JF. Scripta Mater 2007;56, in press, doi:10.1016/j.scriptamat.2007.02.022.
[19] Greer AL, Rutherford KL, Hutchings M. Int Mater Rev 2002;47:87.
[20] Prakash B. Wear 2005;258:217.
[21] Miyoshi K, Buckley DH. Thin Solid Films 1984;118:363.
[22] Wong CJ, Li JCM. Wear 1984;98:45.
[23] Blau PJ. Wear 2001;250:431.
[24] Ma MZ, Liu RP, Xiao Y, Lou DC, Liu L, Wang Q, et al. Mater Sci Eng A 2004;386:326.
[25] Dienwiebel M, Pradeep N, Verhoeven GS, Zandbergen HW, Frenken JWM. Surf Sci 2005;576:197.
[26] Goto H, Uchijo K. Wear 2005;259:613.
[27] Kato H, Hirano T, Matsuo A, Kawamura Y, Inoue A. Scripta Mater 2000;43:503.
[28] Hirano T, Kato H, Matsuo A, Inoue A. Mater Trans JIM 2000;41:1454.
[29] Siegrist ME, Siegfried M, Löffler JF. Mater Sci Eng A 2006;418:236.
[30] Bhushan B. Introduction to tribology. New York: John Wiley and Sons; 2002.
[31] Kishore, Sampathkumaran P, Seetharamu S, Thomas P, Janardhana M. Wear 2005;259:634.
[32] Buzzi S, Jin K, Uggowitzer PJ, Tosatti S, Gerber I, Löffler JF. Intermetallics 2006;14:729.